Electronic Supplementary Information

Highly Efficient and Stable Organic Additive for Positive Electrolyte in Vanadium Redox Flow Battery: Taurine Biomolecule Containing $–NH_2$ and $–SO_3H$ Functional Groups

Jinyeon Hwang,[a] Bo-mi Kim, [a] Joonhee Moon,[b] Asad Mehmood [a] and Heung Yong Ha[a]*

[a] Center for Energy Convergence Research, Green City Technology Institute, Korea Institute of Science and Technology (KIST), Seoul 02792, Republic of Korea

[b] Advanced Nano-surface Research Team, Korea Basic Science Institute (KBSI), Daejeon 34133, Republic of Korea

Corresponding author:

Dr. Heung Yong Ha

Principle Research Scientist

E-mail: hyha@kist.re.kr

Korea Institute of Science and Technology (KIST), Republic of Korea

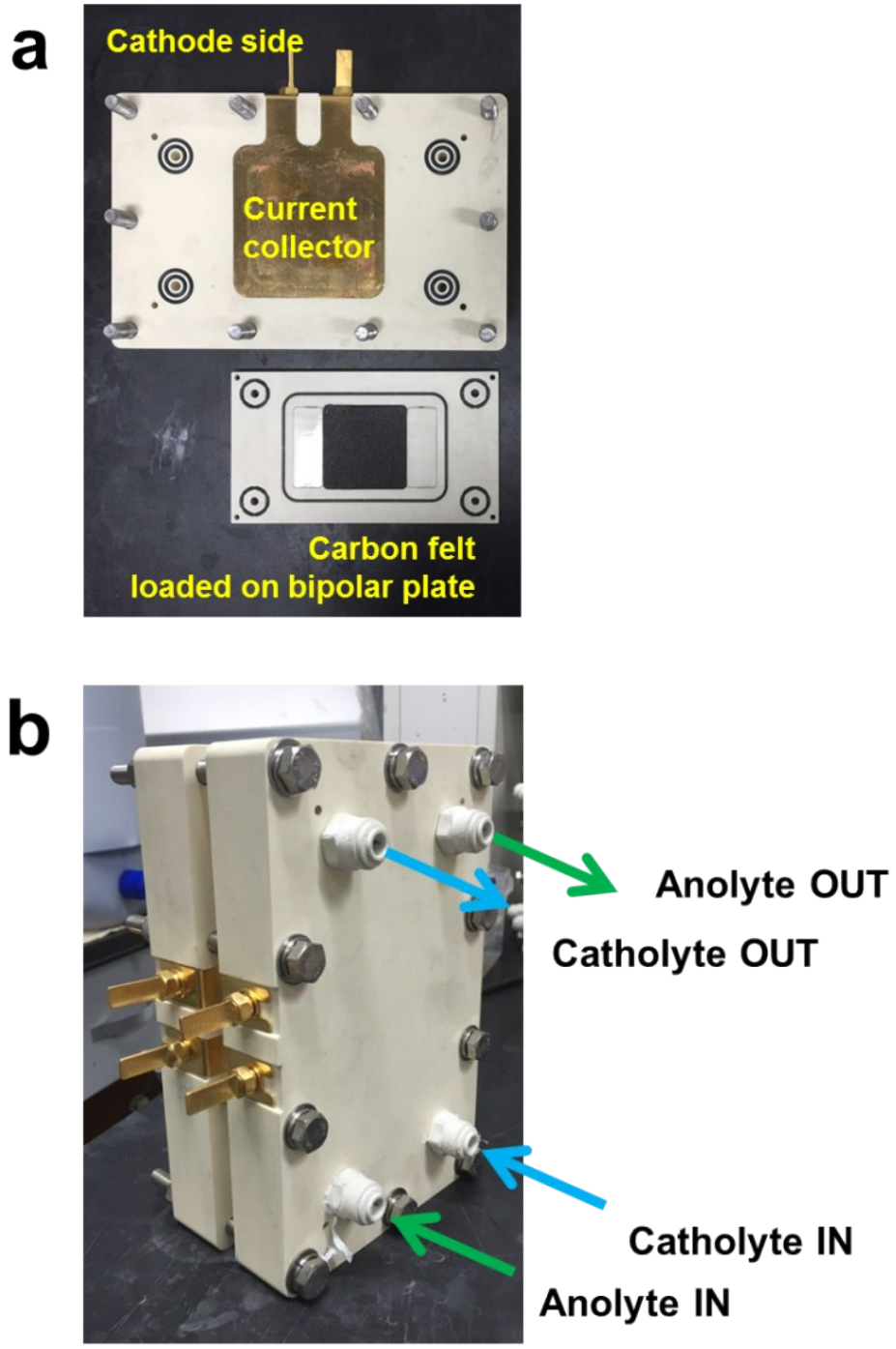

Figure S1. A single cell fixture of VRFB

(a) An endplate consists of a brass current collector attached on a PVC frame and a carbon felt electrode is placed on a graphite bipolar plate that is embedded in a PVC frame. (b) An assembled full cell fixture of VRFB. Anolyte and catholyte are supplied from the bottom and exit to the top through respective ports for efficient wetting of the electrodes.

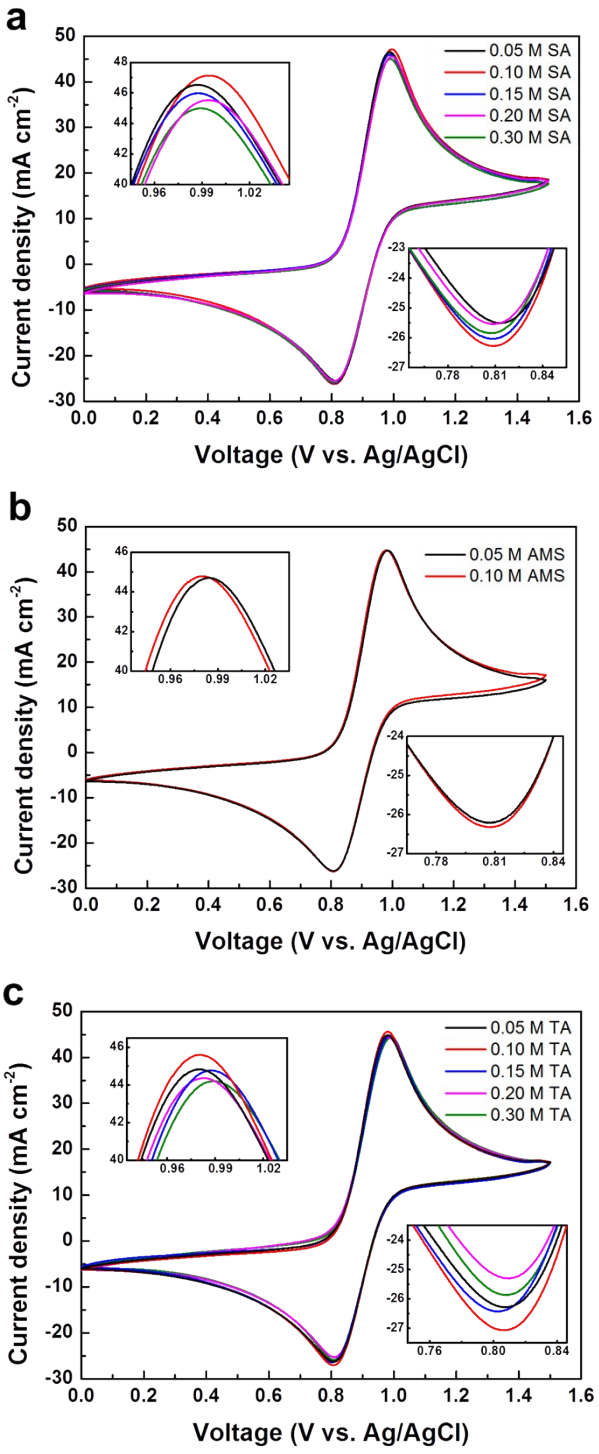

Figure S2. Cyclic voltammetry (CV) analysis with varying concentrations of organic additives

Current density vs. applied potential CV data reveal the concentration dependence of (a) SA, (b) AMS, and (c) TA organic additives in the range of 0.05 M to 0.30 M. Due to the solubility limit of AMS, (0.15 M) its CV data were obtained only in the concentration range from 0.05 M to 0.10 M. Optimized concentration is determined to be 0.1 M based on the maximum current densities and overpotentials (ΔE) obtained at various concentrations.

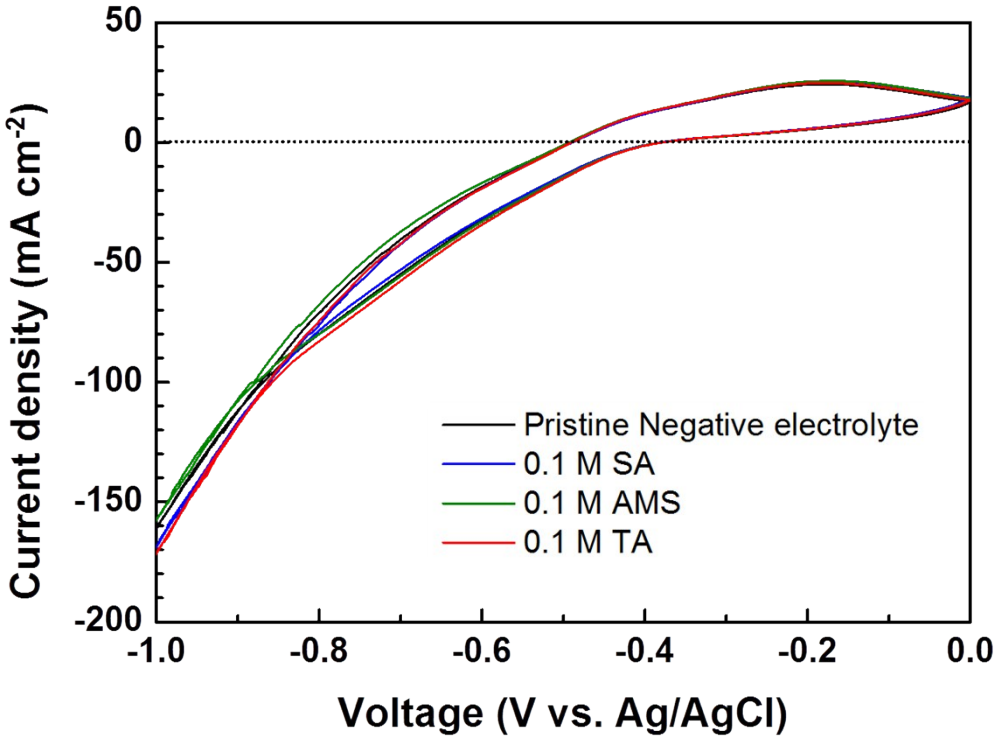

Figure S3. Electrochemical performance of the negative electrolytes containing the additives. Cyclic voltammograms (CV) of the negative electrolytes containing the additives were taken using a three-electrode system. (Working electrode = 1 cm^2 of graphite plate, Counter electrode = Pt plate, Reference electrode = Ag/AgCl) Each additive was added into a 3.0 M sulfuric acid solution containing 1.5 M V^{3+}. The CVs obtained at a rate of 20 mV/sec show that there is no appreciable improvement in terms of overpotential and j_{pa}, j_{pc} values regardless of the additives tested. That is,all the organic additives tested including taurine do not have any effect on the performance of the negative electrolyte. Therefore, it is certain that the improved performance of the VRFB is mainly originated from the activity of taurine in the positive electrolyte.

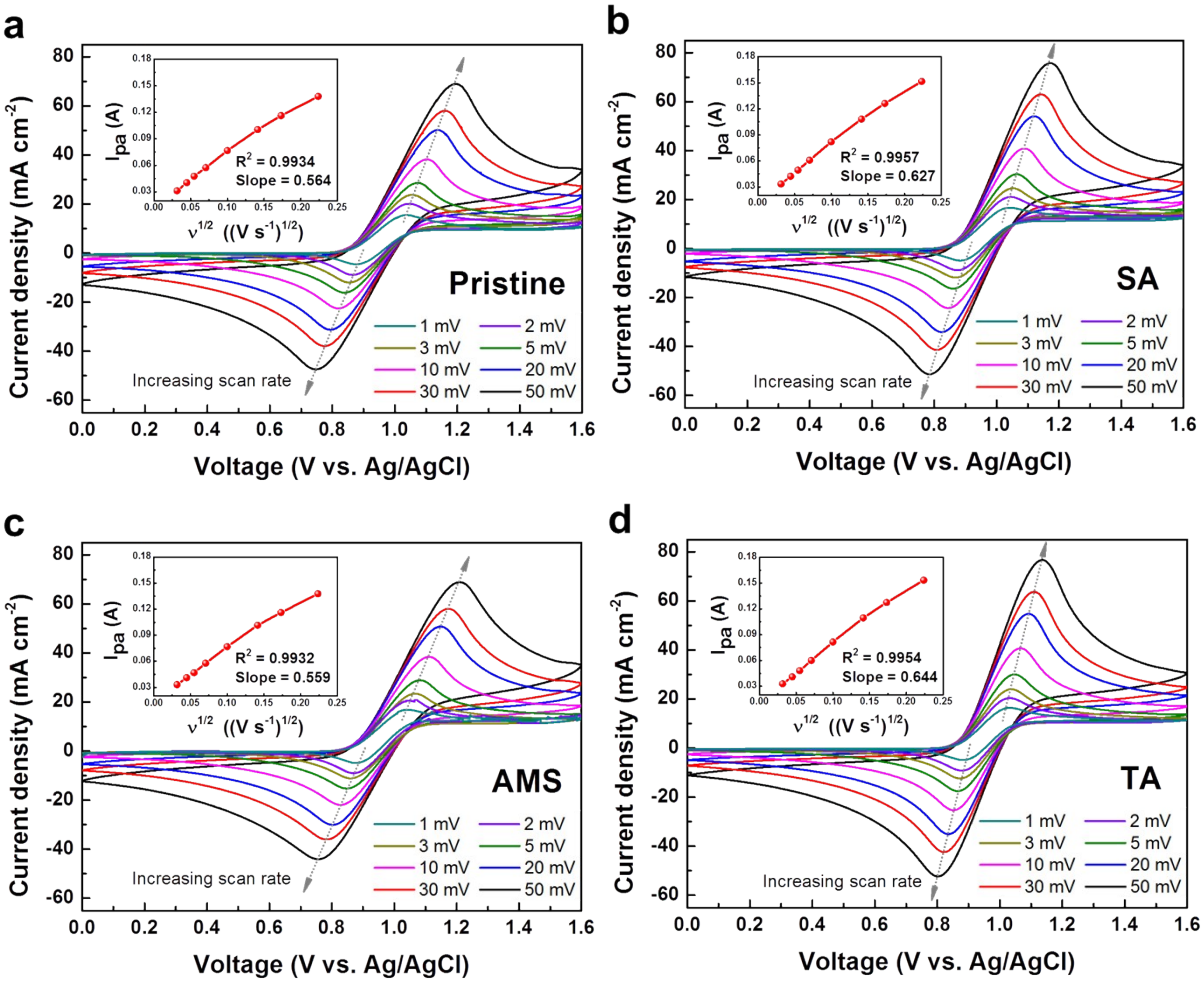

Figure S4. Cyclic voltammograms obtained at different scan rates

CVs of (a) pristine electrolyte, (0.05 M $VOSO_4$/0.1 M H_2SO_4) (b) 0.01 M SA-added, (c) 0.01 M AMS-added, and (d) 0.01 M TA-added electrolyte under different scan rates ranging from 1 mV sec^{-1} to 50 mV sec^{-1}. At higher scan rates, the current densities in the anodic and the cathodic reactions are increased. Insets display the linear correlation between the output current and the root of scan rate, implying that the mass transport rate of vanadium species limits the kinetics of cathodic redox reaction. In addition, the slope of (d) is 14.2% greater than (a), because the TA additive helps to improve the diffusion rate of vanadium ions by bifunctional doping of the electrode. Coefficient of determination (R^2) is notated in the inset of each graph.

	j_{pa} (mA cm^{-2})	j_{pc} (mA cm^{-2})	I_{pa}/I_{pc}	E_{pa} (V)	E_{pc} (V)	ΔE (mV)
Pristine	**50.19**	**-43.03**	**1.17**	**1.14**	**0.79**	**346**
0.1 M SA	**54.05**	**-46.57**	**1.16**	**1.12**	**0.82**	**297**
0.1 M AMS	**50.77**	**-42.58**	**1.19**	**1.15**	**0.80**	**345**
0.1 M TA	**54.76**	**-47.56**	**1.15**	**1.09**	**0.84**	**257**

Table S1. Summary of the cyclic voltammetry (CV) parameters of the electrolytes with 0.1 M organic additives

The anodic peak current density, (j_{pa}) cathodic peak current density, (j_{pc}) the ratio between the anodic versus the cathodic output current, (I_{pa}/I_{pc}) oxidation peak potential, (E_{pa}) reduction peak potential, (E_{pc}) and the potential gap between vanadium redox potentials (ΔE) of VRFB positive electrolyte (1.5 M $VOSO_4$/3.0 M H_2SO_4) with or without an organic additive. Each current density was calculated based on the extrapolated background baselines which were calibrated using Nicholson equation. [1-2]

	R_{ohm} (mΩ)	R_{ct} (mΩ)	CPE			Fitting χ^2 (10^{-3})
			Y_0 (10^{-3})	n	C (mF)	
Pristine	**751.1**	**145.9**	**79.5**	**0.9961**	**78.1**	**2.918**
0.1 M SA	**724.6**	**111.8**	**193.2**	**0.9956**	**190.0**	**2.461**
0.1 M AMS	**758.3**	**167.2**	**90.6**	**0.9959**	**89.1**	**2.790**
0.1 M TA	**711.7**	**85.5**	**133.6**	**0.9958**	**131.1**	**1.984**

Table S2. Electrochemical AC impedance analysis (EIS) parameters of the electrolytes

Ohmic resistance, (R_{ohm}) charge transfer resistance, (R_{ct}) CPE values, (Y_0, n, C) and X^2 (chi-square) values of the electrolytes with or without organic additives were calculated from the EIS data. The lower R_{ct} indicates faster charge transfer kinetics. CPE factors are influenced by the electrical double layer capacitance. For instance, high Y_0 value means high electrical double layer capacitance at the electrode/electrolyte interface, which is advantageous for vanadium redox reaction. X^2 factors less than 0.01 indicate that the simulated fitting line in Figure 2d is reliable. [3-5]

a

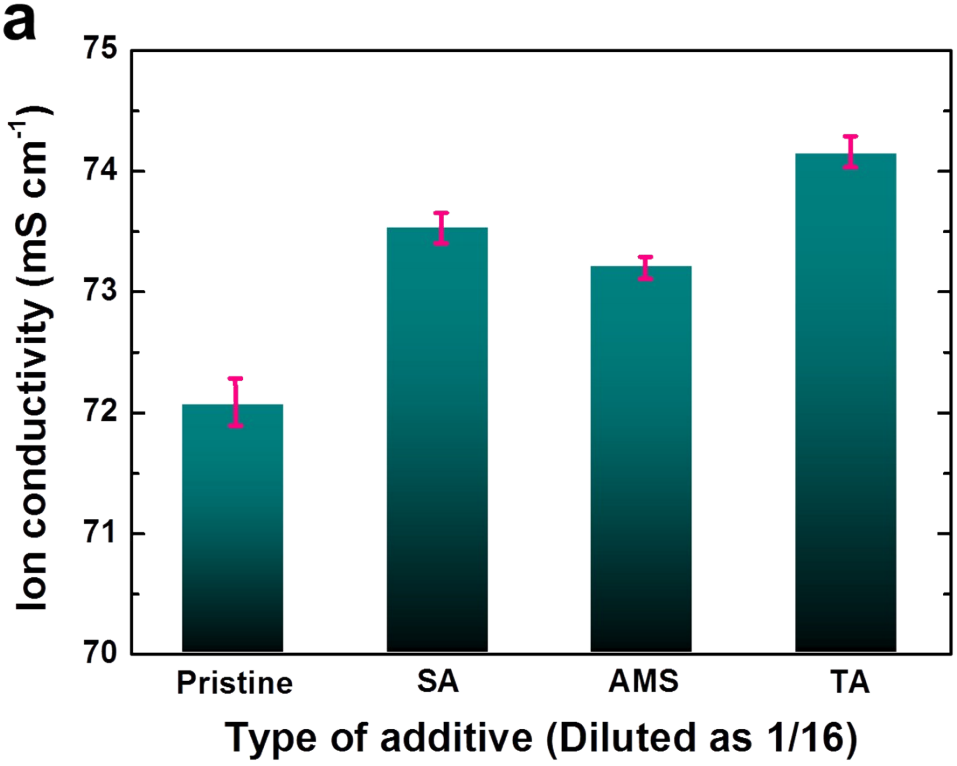

b

	1.5 M Vanadium / 3.0 M H_2SO_4	With 0.1 M SA	With 0.1 M AMS	With 0.1 M TA
V^{3+} (III)	9.30 cP (at 20.6℃)	-	-	-
VO^{2+}(IV)	7.89 cP (at 20.8℃)	7.93 cP (at 20.7℃)	8.02 cP (at 20.8℃)	7.98 cP (at 20.7℃)
VO_2^+(V)	6.84 cP (at 20.7℃)	-	-	-

Figure S5. Ion conductivity and viscosity data for the electrolytes

a, Ion conductivity measured by conductivity meter (Thermo Orion) using 1/15 diluted VO^{2+}(IV) solution. By adding additives, the conductivity is slightly increased above the error range. **b,** Viscosity data depending on the type of vanadium ion and additives. Additives increase the viscosity, however, the amount of change is small. (0.5 ~ 1.6% of pristine solution)

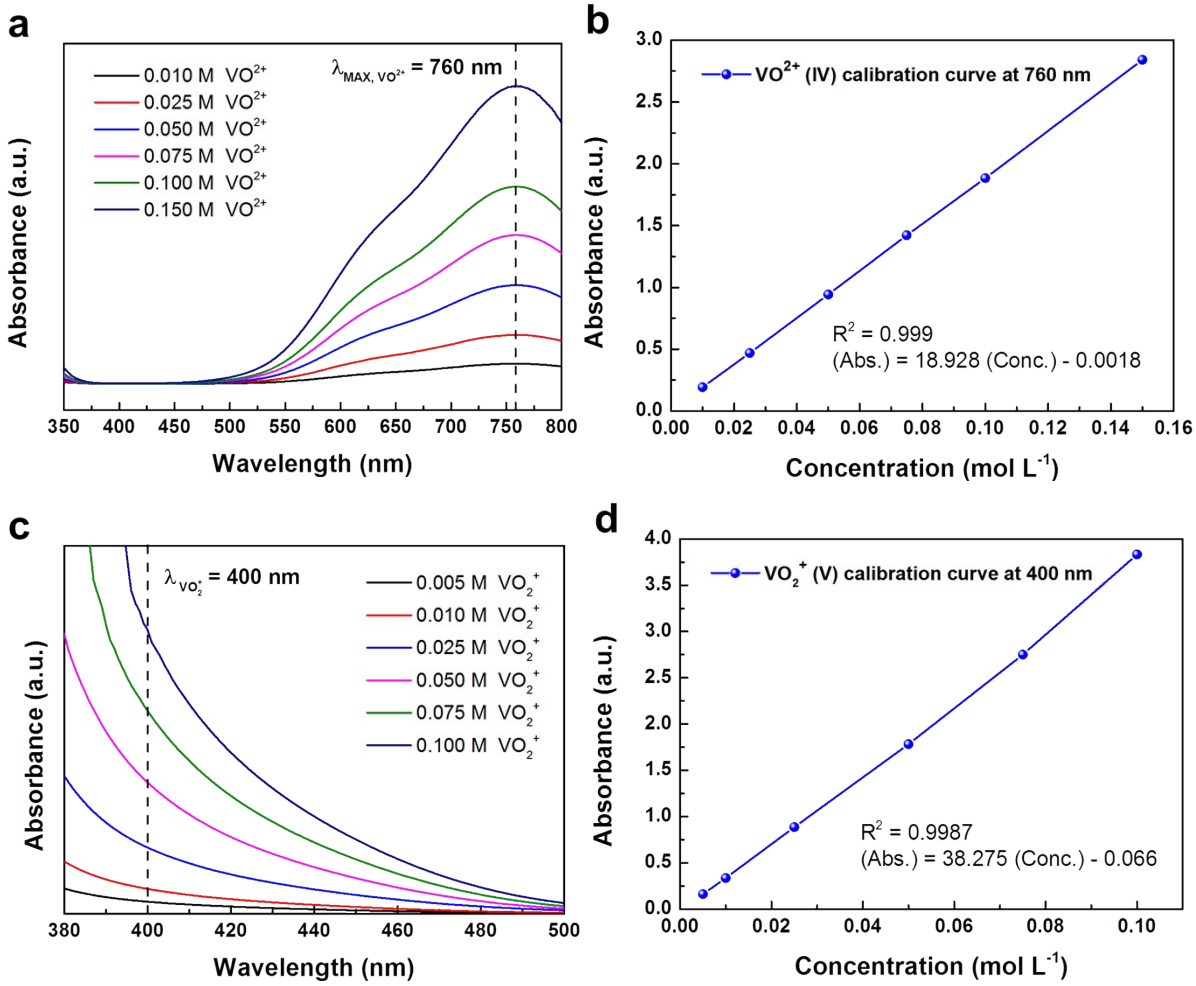

Figure S6. UV-Visible spectra and calibration curves of VO^{2+}(IV) and VO_2^+(V)

UV-Visible spectra were measured with various concentrations of (a) VO^{2+}(IV) and (c) VO_2^+(V). Each standard vanadium solution was prepared using 3.0 M sulfuric acid as a supporting electrolyte. During the scanning from 300 nm to 800 nm, VO^{2+}(IV) showed maximum absorbance at 760 nm. (λ_{max}) On the other hand, VO_2^+(V) did not show stable absorbance at λ_{max} so that relatively stable absorbance at 400 nm was utilized as a standard wavelength to calibrate the concentration. From Beer's law [6], the calibration curves of (b) VO^{2+}(IV) and (d) VO_2^+(V) were obtained. Each calibration curve shows high reproducibility and high accuracy. The correlation equations between absorbance and concentration are notated in the graphs with its R^2 value.

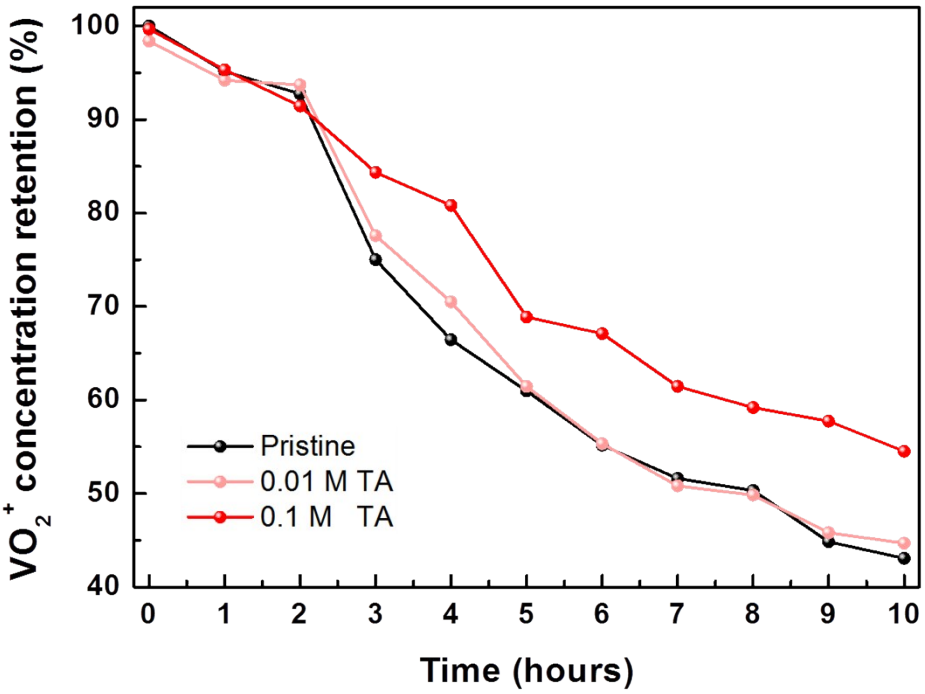

Figure S7. Thermal stability of VO_2^+(V) ion depending on the taurine concentration

At 40°C, the concentrations of VO_2^+(V) in the electrolytes with and without taurine additive were measured starting from 1.5 M of initial concentration. Compared to the pristine electrolyte, the electrolyte with 0.1 M taurine shows improved thermal stability.

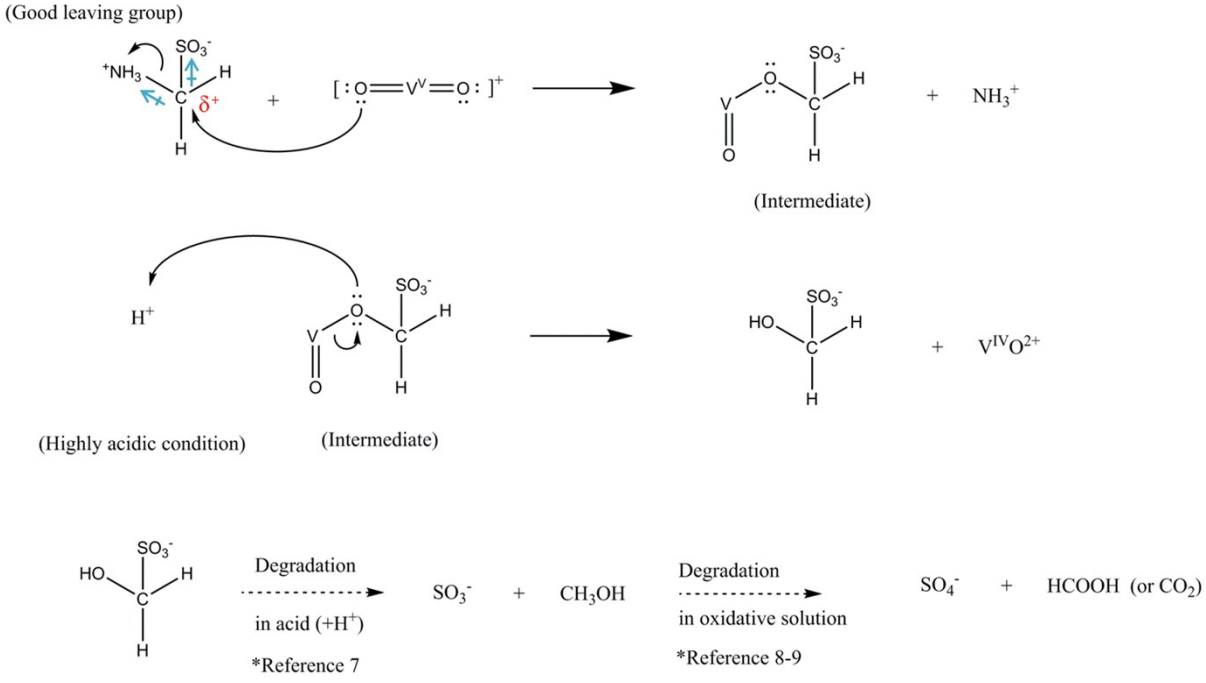

Figure S8. A tentative mechanism of the chemical degradation of AMS by VO_2^+(V)

Electronegative $–NH_3^+$ and $–SO_3^-$ functional groups make the central carbon atom of AMS partially positive. (δ^+) This strong inductive effect induces a nucleophilic substitution reaction. Since the protonated amine group is a good leaving group, it can be easily detached from the carbon of AMS when it interacts with oxidative vanadium ions. [10-11] This oxidation of AMS in turn reduces VO_2^+(V) to VO^{2+}(IV). (Reducing agent) Additionally, the central carbon of AMS can also be attacked by HSO_4^- or SO_4^{2-} because of the high concentration (~ 3.0 M) of nucleophiles. (HSO_4^-, SO_4^{2-}) [12-13]

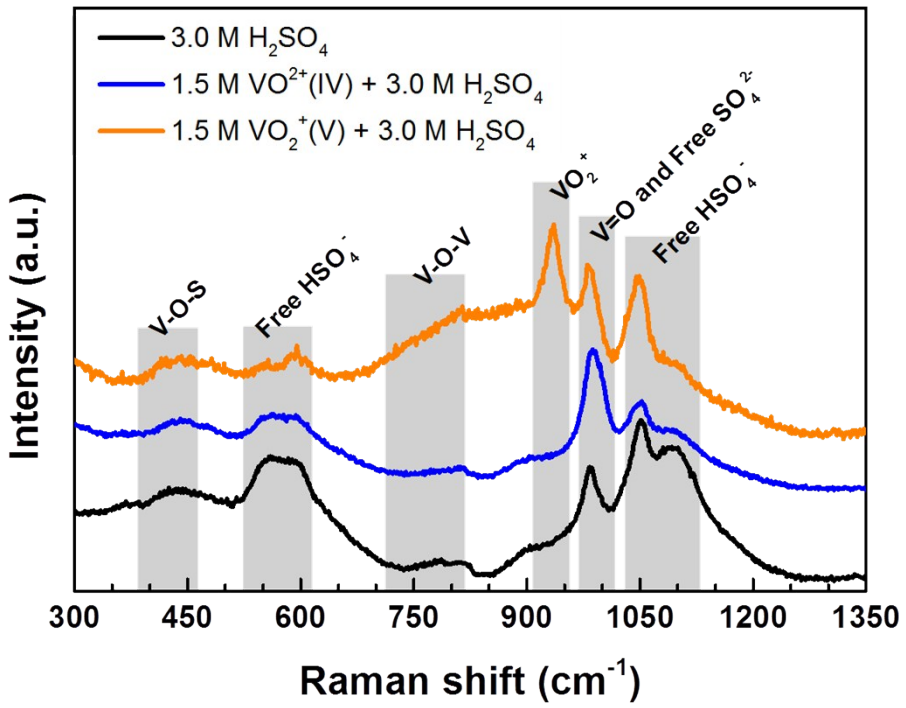

Figure S9. Raman spectra of the reference electrolytes

3.0 M sulfuric acid showed the highest free HSO_4^- Raman peak at 520 ~ 610 cm^{-1} and 1030 ~ 1100 cm^{-1}, indicating that there are large amounts free bisulfate ions without any vanadium coordination. At 720 ~ 800 cm^{-1}, a broad peak of vanadium dimer (V-O-V bridged $V_2O_3^{3+}$) was detected, which is generally found in VO_2^+(V) solution. In addition, VO_2^+(V) showed its characteristic Raman peak at 930 ~ 940 cm^{-1} generated by its symmetrical stretching. The peak at 980 ~ 1020 cm^{-1} was the overlapped Raman peak with terminal vibration of V=O oxygen and symmetrical stretching of free sulfate (SO_4^{2-}). [14]

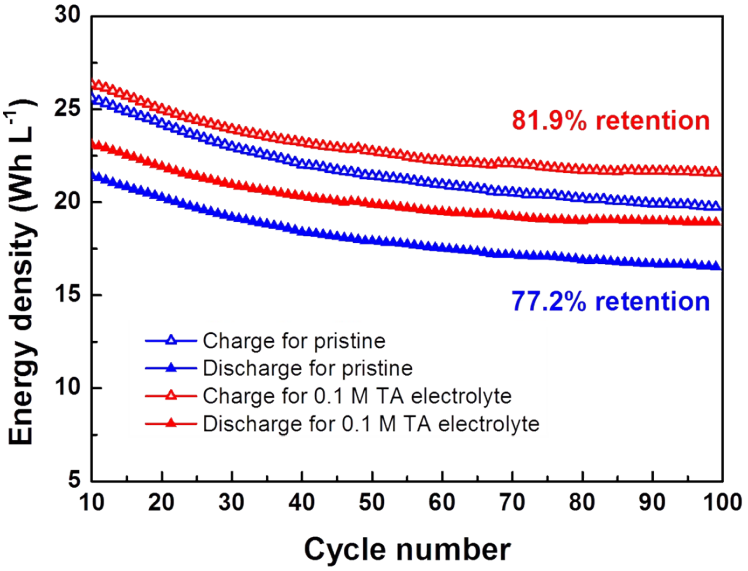

Figure S10. Energy density retentions during 100 cycles of VRFB operations

After 100 cycles, the electrolyte with 0.1 M taurine showed 81.9% energy density retention compared to the initial value whereas the pristine electrolyte without TA showed only 77.2% of retention. The high energy density retention of the TA electrolyte is caused by improved reversibility and depressed crossover of vanadium ions.

	Pristine (without taurine)			0.1 M Taurine electrolyte		
	C.E.	V.E.	E.E.	C.E.	V.E.	E.E.
50 mA cm^{-2}	95.17	89.27	84.96	96.46	91.08	87.86
75 mA cm^{-2}	95.05	84.54	80.36	96.69	86.97	84.09
100 mA cm^{-2}	96.02	79.79	76.62	96.93	82.93	80.39
125 mA cm^{-2}	97.04	74.78	72.57	97.20	78.98	76.78
150 mA cm^{-2}	98.29	69.30	68.11	97.52	75.09	73.22

Table S3. VRFB efficiencies at different current densities

From 50 to 150 mA cm^{-2}, current efficiency (C.E.), voltage efficiency (V.E.), and energy efficiency (E.E.) were calculated with or without 0.1 M of taurine additive. All efficiencies are averaged values obtained during at least three cycles of charge-discharge measurement shown in Figure 5a using the same VRFB cell.

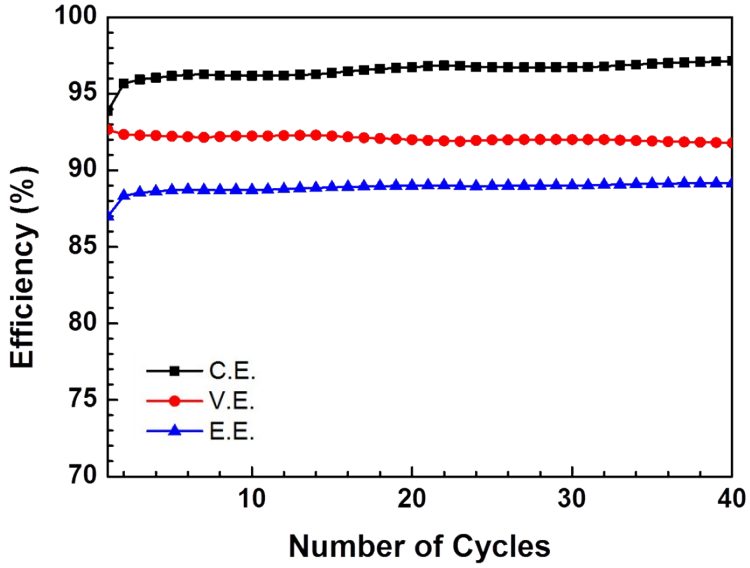

Figure S11. A reproducibility test with a TA-containing electrolyte (40 cycles)

At 50 mA cm^{-1}, The 0.1 M TA-electrolyte showed reproducible results that are comparable to the data in Table S3. Averaged-out columbic efficiency, voltage efficiency, energy efficiency over the 40 cycles are 96.51%, 92.08%, 88.87%, respectively.

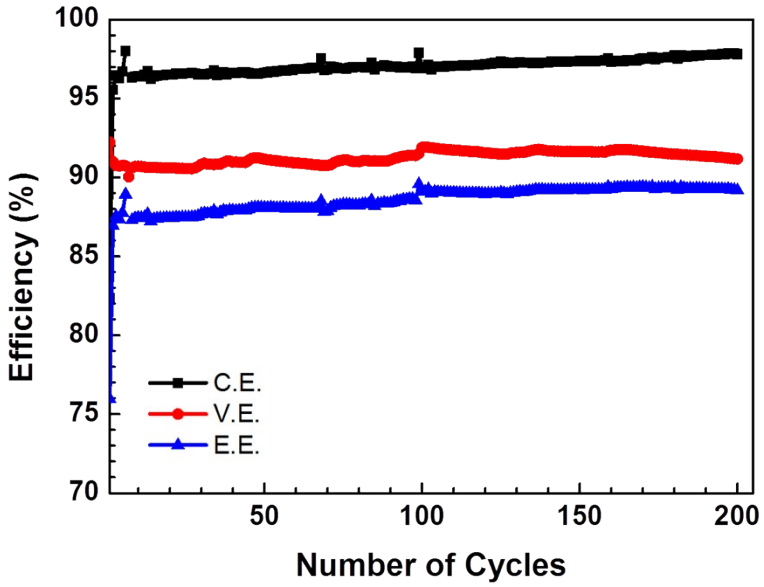

Figure S12. A long-term cell test with a TA additive (200 cycles)

At 50 mA cm^{-1}, 0.1 M TA-electrolyte showed stable cell performance during 200 cycles. Averaged-out columbic efficiency, voltage efficiency, energy efficiency over the cycle are 96.88%, 90.64%, 87.81%, respectively. The chemical degradation of TA was not detected after the cell operation.

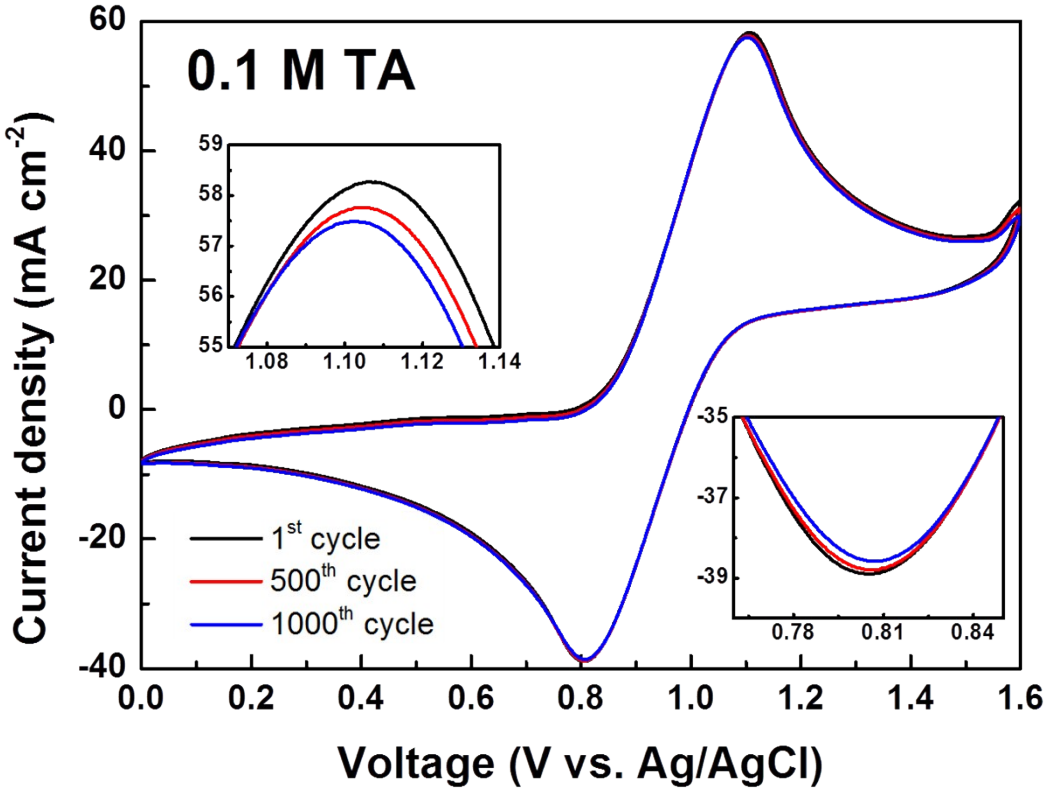

Figure S13. Stability of taurine additive by a long-term cyclic voltammetry (CV) test

CV curves at the 1st, 500th, and 1,000th cycle from 0.0 V to 1.6 V. (Scan rate = 20 mV sec^{-1}) During 1,000 cycles of CV operation, negligible degradation was detected in terms of current density and overpotential. (0.98 mA cm^{-2} of j_{pa}, 0.04 mA cm^{-2} of j_{pc}, and 0.08 V of ΔE were decreased after 1,000 cycles) Left top inset shows anodic peaks and right bottom shows cathodic peaks.

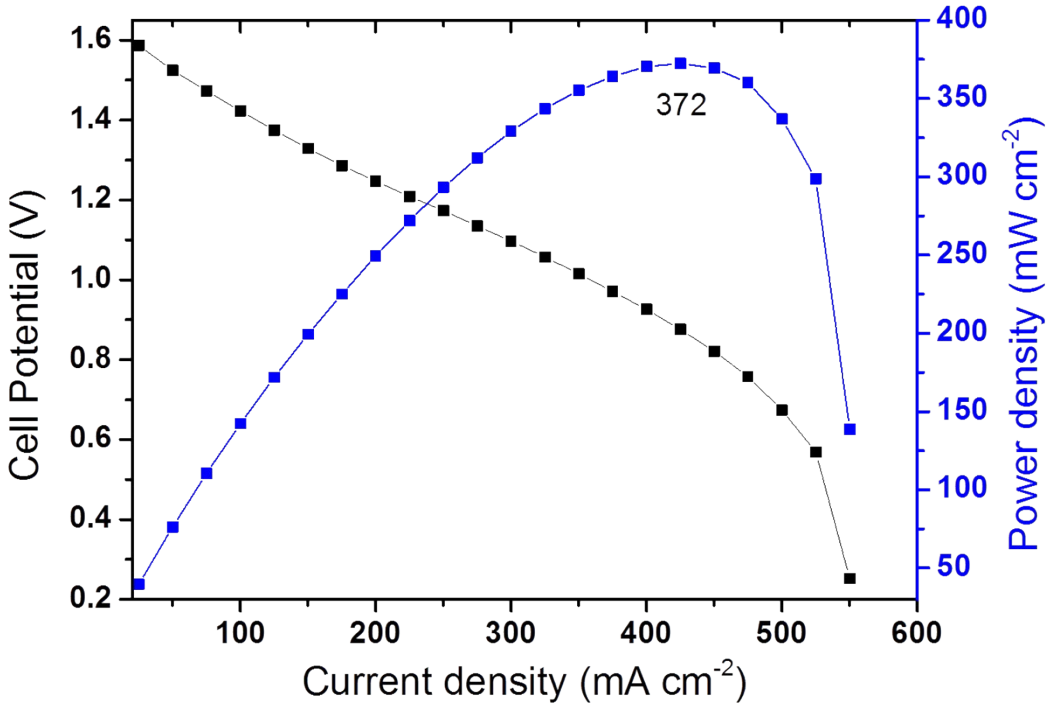

Figure S14. VRFB cell polarization curves

From 0% to 100% SOC, the cell potential and power density were measured by changing current density. Measured peak power density was 372.3 mW cm^{-2} at 425 mA cm^{-2}. From the slope of linear region in I-V curve, the cell resistance was calculated as 65.9 mΩ.

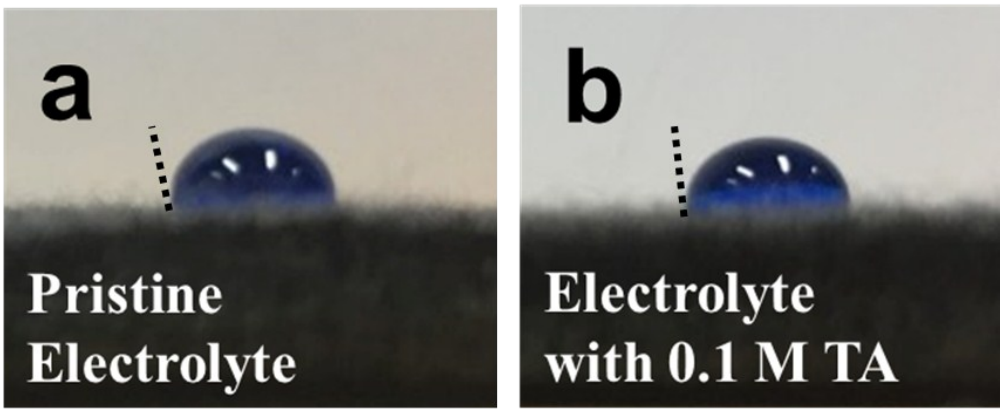

Figure S15. Contact angle measurement using vanadium electrolytes on the fresh carbon felts

For checking the wettability before the cell test, the VO^{2+}(IV) electrolyte (a) without and (b) with 0.1 M TA was dropped onto the fresh carbon felt electrode. Even though the contact angle is slightly reduced in (b), the difference is negligible.

Type	Additive	Conc. (M)	Cycle number	Current density (mA cm^{-2})	EE (%)	Discharge capacity retention (%)	Ref.
–OH group	Glucose	~ 0.08	—	20	70.4	—	[15]
	Fructose	~ 0.08	—	20	67.6	—	[15]
	Mannitol	~ 0.08	—	20	76.2	—	[15]
	D-Sorbitol	~ 0.08	—	20	81.8	—	[15]
	Inositol	0.054	20 (50)	30	81.5	87 (67.5)	[16]
	Glycerol / n-propyl alcohol	0.14 / 0.13	—	—	—	—	[17]
–NH_2/ –COOH group	L-Aspartic acid	0.06	40 (50)	60	76.4	85 (81.3)	[18]
	L-Glutamic acid	~ 0.10	40 (50)	60	75.9	88.4 (85.5)	[19]
–NH_2/ –SO_3H group	Sulfamic acid	3.0	50	20	84.57	(86)	[20]
	Aminomethane sulfonic acid	0.02	40 (50)	40	81.5	82.7 (78.4)	[21]

Table S4. Performance comparison of the VRFBs employing various types of organic additives

In Table S4, the effects of various organic additives on the performance of VRFB are summarized. To compare the capacity retention in the same condition, the retention after 50 cycles is used. Unreported data are notated as a dash mark, and estimated values are parenthesized.

		Pristine carbon felt	Carbon felt after 100 cycles with 0.1 M TA
Carbon (total)		**64.54 at%**	**54.61 at%**
C-C	**284.6 eV**	**(77.7 %)**	**(73.6 %)**
C-N	**285.9 eV**	**-**	**(10.0 %)**
C-O	**286.8 eV**	**(11.3 %)**	**(5.4 %)**
C-S	**287.7 eV**	**-**	**(3.0 %)**
C=O	**288.8 eV**	**(6.3 %)**	**(5.3 %)**
O-C=O	**291.0 eV**	**(4.7 %)**	**(2.7 %)**
Nitrogen (total)		**0.00 at%**	**2.71 at%**
Pyridinic	**400.0 eV**	**-**	**(12.4 %)**
Pyrrolic	**400.6 eV**	**-**	**(27.1 %)**
Graphitic	**401.8 eV**	**-**	**(60.5 %)**
Sulfur (total)		**0.00 at%**	**6.27 at%**
S $2p_{3/2}$	**168.9 eV**	**-**	**(66.7 %)**
S $2p_{1/2}$	**170.1 eV**	**-**	**(33.3 %)**
Oxygen (total)		**35.46 at%**	**36.41 at%**

Table S5. XPS data of the carbon felt before and after the cycling test

Bonding states are denoted with their specific binding energies. Elemental composition of C, N, O, S atoms and the composition of each bonding type are summarized in the table.

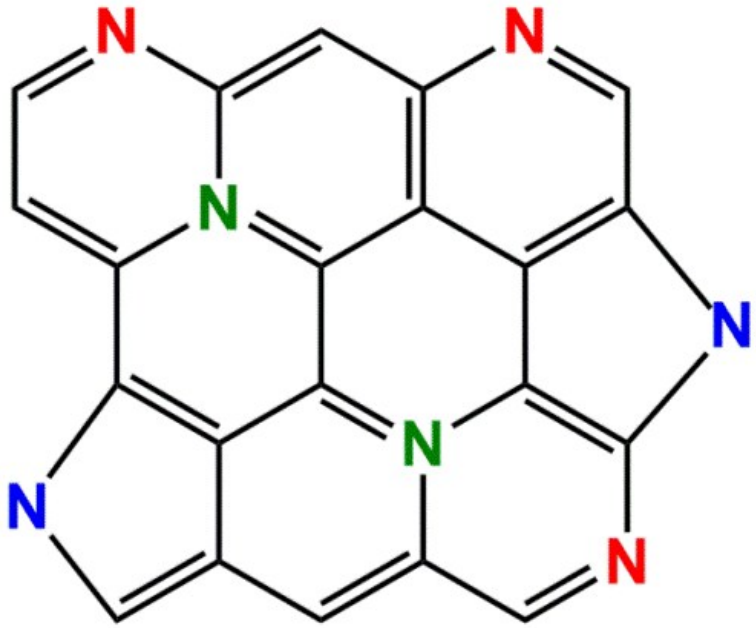

Figure S16. Different doping sites of nitrogen

Red, blue, and green colored nitrogens (N) indicate pyrinidic, pyrrolic, and graphitic sites, respectively. sp^3-hybridized pyridinic and pyrrolic nitrogens are located at the carbon edge sites. On the other hand, sp^2-hybridized graphitic nitrogens are located on the basal plane.

References

[1] R. S. Nicholson and I. Shain, *Anal. Chem*., 1964, **36**, 706-723.

[2] J. H. Park, J. J. Park, O. O. Park, C.-S. Jin and J. H. Yang, *J. Power Sources*, 2016, **310**, 137-144.

[3] X. Wu, S. Liu, N. Wang, S. Peng and Z. He, *Electrochim. Acta*, 2012, **78**, 475-482.

[4] Y. Shao, X. Wang, M. Engelhard, C. Wang, S. Dai, J. Liu, Z. Yang and Y. Lin, *J. Power Sources,* 2010, **195**, 4375-4379.

[5] C.-N. Sun, F. M. Delnick, D. S. Aaron, A. B. Papandrew, M. M. Mench and T. A. Zawodzinski Jr., *J. Electrochem. Soc.*, 2013, **160**, A973-A979.

[6] N. H. Choi, S.-K. Kwon and H. Kim, *J. Electrochem. Soc*., 2013, **160**, A973-A979.

[7] C. Qi, X. Liu, Y. Li, C. Lin, J. Ma, X. Li and H. Zhang, *J. Hazardous Materials*, 2017, **328**, 98-107.

[8] M. E. Scofield, C. Koenigsmann, L. Wang, H. Liu and S. S. Wong, *Energy Environ. Sci*., 2015, **8**, 350-363.

[9] K.-I. Ota, Y. Nakagawa, M. Takahashi, *J. Electroanal. Chem*, 1984, **179**, 179-186

[10] P. Jaramillo, L. R. Domingo and P. Perez, *Chem. Phys. Lett.,* 2006, **420**, 95-99.

[11] M. Paborji, W. N. Waugh and V. J. Stella, *J. Pharmaceutical Sci*., 1987, **76**(2), 161-165.

[12] R. Shapiro, R. E. Servis and M. Welcher, *J. Am. Chem. Soc*., 1970, **92**, 422-424.

[13] W. V. Cohen, *J. Org. Chem*., 1961, **26**, 4021-4026

[14] N. Kausar, R. Howe and M. Skyllas-Kazacos, *J. Appl. Electrochem.*, 2001, **31**, 1327-1332.

[15] S. Li, K. Huang, S. Liu, D. Fang, X. Wu, D. Lu and T. Wu, *Electrochim. Acta*, 2011, **56**, 5483-5487.

[16] X. Xu, S. Liu, N. Wang, S. Peng and Z. He, *Electrochim. Acta*, 2012, **78**, 475-482.

[17] Z. Jia, B. Wang, S. Song and X. Chen, *J. Electrochem. Soc*., 2012, **159**, A843-A847.

[18] J. Liu, S. Liu, Z. He, H. Han and Y. Chen, *Electrochim. Acta*, 2014, **130**, 314-321.

[19] Y. Lei, S.-Q. Liu, C. Gao, X.-X. Liang, Z.-X. He, Y.-H. Deng and Z. He, *J. Electrochem., Soc.*, 2013, **160**, A722-A727.

[20] Z. He, Y. He, C. Chen, S. Yang, J. Liu, Z. He and S. Liu, *Ionics*, 2014, **20**, 949-955.

[21] Z. He, J. Liu, H. Han, Y. Chen, Z. Zhou, S. Zheng, W. Lu, S. Liu and Z. He, *Electrochim. Acta*, 2013, **106**, 556-562.